The Canadian Mineralogist
Vol. 43, pp. 1157-1170 (2005)

CHARACTERIZATION OF ALUMINUM-RICH PHASES IN HEAP-LEACH PADS AT THE LANDUSKY GOLD MINE, MONTANA, USA

NIKOLAY V. SIDENKO[§] AND BARBARA L. SHERRIFF

Department of Geological Sciences, University of Manitoba, Winnipeg, Manitoba R3T 2N2, Canada

HEATHER E. JAMIESON

Department of Geological Sciences and Geological Engineering, Queen's University, Kingston, Ontario K7L 3N6, Canada

SHANNON C. SHAW

Robertson GeoConsultants Inc., Suite 330, 580 Hornby Street, Vancouver, British Columbia V6C 3B6, Canada

ABSTRACT

Hydrothermal alteration, pre-mining weathering, mining, metal extraction by heap leaching with cyanide, and post-mining alteration of rock at the Landusky gold mine, in Montana, have resulted in repeated transformations of Al-bearing minerals and their eventual dissolution to form Al-rich aqueous solutions. The primary aluminosilicate minerals in the Landusky syenite are K-feldspar and sodic plagioclase. Detailed studies of clay mineralogy and geochemistry have shown that these feldspars were partially altered to illite during hydrothermal alteration of the syenite, probably coincidental with the gold-mineralization event. Kaolinite was formed by weathering of illite and feldspars. Then alkaline conditions (pH >10) during cyanide leaching (1979–1996) caused the hydrothermal illite to become laced with a smectite (the K-dominant analogue of beidellite), which is stable under alkaline conditions. After the mine closed, oxidation of pyrite decreased the pH, and the smectite became unstable, forming kaolinite. Over time, further increases in acidity resulted in the dissolution of kaolinite, thereby generating elevated concentrations of Al in the drainage water (up to 100 mg/L). Precipitation of amorphous aluminum hydroxides and oxyhydroxides from this water resulted in the blockage of drainage pipes, and a reduced efficiency of a treatment plant installed to remove cyanide, selenium and nitrate.

Keywords: cyanide heap-leach, acid rock-drainage (ARD), aluminum, smectite, K-dominant analogue of beidellite, illite, kaolinite, feldspar dissolution, Landusky gold mine, Montana.

SOMMAIRE

L'altération hydrothermale, les altérations de surface avant le début des opérations minières, l'exploitation minière, l'extraction des métaux par lixiviation en tas avec cyanure, et l'altération subie depuis l'activité minière à la mine d'or de Landusky, au Montana, ont causé des transformations répétées impliquant les minéraux d'aluminium, et leur dissolution éventuelle pour former des solutions aqueuses riches en Al. Les aluminosilicates primaires dans la syénite de Landusky sont le feldspath potassique et l'albite. Des études détaillées de la minéralogie des argiles et de la géochimie ont montré que ces feldspaths ont été partiellement transformés en illite lors de l'altération hydrothermale de la syénite, probablement au temps de la minéralisation aurifère. La kaolinite est ensuite apparue par météorisation de l'illite et des feldspaths. Vient ensuite la lixiviation au cyanure sous conditions alcalines (pH >10) entre 1979 et 1996, qui a provoqué le remplacement de l'illite hydrothermale par une smectite (l'analogue à dominance de K de la beidellite), rendue stable. Après la fermeture de la mine, l'oxydation de la pyrite a causé une diminution du pH, et la smectite est devenue instable, à la faveur de la kaolinite. Avec le passage du temps, l'acidité a continué d'augmenter, causant la dissolution de la kaolinite, et ainsi les concentrations élevées en Al dans l'eau de drainage (jusqu'à 100 mg/L). La précipitation d'hydroxydes et d'oxyhydroxydes d'aluminium dans cette eau est responsable du bloquage des tuyaux de drainage, et d'une efficacité réduite des installations prévues pour le traitement des eaux afin d'en éliminer le contenu en cyanure, sélénium et nitrate.

(Traduit par la Rédaction)

Mots-clés: lixiviation en tas au cyanure, drainage d'eaux de mine acides, aluminium, smectite, analogue à dominance de K de la beidellite, illite, kaolinite, dissolution des feldspaths, mine d'or de Landusky, Montana.

§ *E-mail address*: sidenkon@cc.umanitoba.ca

Introduction

Cyanide heap-leaching under highly alkaline conditions (pH ≈ 10) is a common method of recovering gold from non-refractory ores. The costs are relatively low, allowing the economic recovery of gold from low-grade deposits. In most cases, environmental impacts are minimized by measures taken to ensure that residual cyanide degrades to non-toxic forms. Upon closure, heap-leach pads are either actively rinsed or passively diluted with meteoric water, so that near-neutral conditions are re-established. Most heap-leach operations involve oxide-rich ore, but if sulfide-rich material (such as pyrite) is present in the rock piles or heaps, then acid may be generated by sulfide oxidation. As an example, at the Summitville gold mine, Colorado, USA, sulfide waste-rocks generated acidic solutions with high concentrations of Al, Cu, Fe, Mn, and Zn, which caused pollution of the Alamosa River (Ortiz *et al*. 1995, Walton-Day *et al*. 1995). In acid-generating mine wastes, aluminum is released from aluminosilicates. The nature of the aluminosilicate minerals is one of the parameters determining the rate of mineral dissolution and, consequently, supply of Al into the drainage water (Jambor & Blowes 1998). In acidic mine-drainage at pH > 4.5, the concentration of Al is controlled by the precipitation of gibbsite and kaolinite (Nordstrom 1982, Nordstrom & Ball 1986, Blowes & Jambor 1990, Blowes *et al*. 1991, Blowes & Ptacek 1994).

In this study, we characterize the Al-bearing phases in samples from two heap-leach pads at the Landusky gold mine, Montana, USA, where unexpectedly high concentrations of Al were found in the drainage water and the precipitation of Al-bearing phases caused problems for the bioreactor installed to remove cyanide, selenium and nitrate.

Background

The Landusky – Zortman gold mines, located in the Little Rocky Mountains, Montana (Fig. 1), exploited Au–Ag deposits in veins of pyrite, iron oxides, jarosite and clay minerals hosted in a syenite and monzonite porphyry (Wilson & Kyser 1988). The first mill was built in 1904, and underground mining continued intermittently to the 1970s. Open-pit mining and heap-leach operations began in 1979 and continued until 1996, when the operating company declared bankruptcy. The site, consisting of ten large leach-pads and a complex water-management system, has been described previously (Shaw & Robertson 2001). Here, the term *leach pad* is used to describe the leached rock material. In this study, we focus on two large, partially conjoined pads that exhibit complex and changing composition of water. The processing of the first pad (L87) started in 1987, and the second (L91), in 1991 (Fig. 1). At some point during the final years of the operations, these pads were physically combined into one very large leach-pad when blasted ore was placed between them, but the independent drainage and water management of each were retained.

During gold-recovery operations, the heap-leach pads were operated at pH ≈ 10. After operations ceased, the leach pads were rinsed with meteoric water, which decreased the pH to near-neutral conditions. The waters draining the pads were then dispersed in a Land Application Disposal program. Over the period 1997–2000, the pH of the water draining the leach pads continued to decrease (Shaw 2000, Shaw & Robertson 2001). Geochemical characterization studies in 1999–2000 involved acid–base accounting and leaching tests of surface samples and drill cuttings, as well as monitoring of oxygen at various depths within the leach pad (Shaw 2000, Shaw & Robertson 2001). The results indicated that: (i) a significant proportion of the spent ore is considered to be potentially acid-generating, (ii) zones of localized acidity have developed within the leach pad (paste pH values of drill cutting ranged from 2 to 8), (iii) substantial quantities of soluble precipitates exist at the surface and at depth in the leach pads, and (iv) oxygen supply is not limited within the leach pad. The quality of water draining the L87 and L91 leach pads has deteriorated over time, such that treatment of the effluent became necessary before disposal. A bioreactor facility was built in 2000 to reduce the cyanide, selenium and nitrate content of the drainage water. In the summer of 2000, concentrations of dissolved Al were 25 mg/L in L87 and 13 mg/L in L91 pads (Applied Biosciences Corporation 2001), whereas the sulfate content was approximately 4500 mg/L for the water of both pads. These concentrations of Al were higher than those used in the bioreactor bench-scale studies. As a result, an Al-rich precipitate formed in the bioreactor tanks, producing high turbidity and reducing efficiency. The results of our mineralogical and geochemical study help in understanding the processes that control the release and attenuation of Al within the leach pads.

Methods of Investigation

Materials

In August 2002, samples of unleached syenite were collected from a newly blasted area at the top of the Gold Bug Butte open pit at the Landusky mine (R6, R7, R15, R18). The samples were selected to reflect different stages of alteration prior to cyanide leaching: unaltered, hydrothermally altered, and weathered. Samples of leached rocks were collected from pits 3 m deep, excavated in the L87 and L91 pads with a backhoe (Table 1). A solid sample (F3) was also obtained of a precipitate that had blocked a pipe used for draining water from leach pad L87.

Aluminosilicate minerals were separated from surface areas of rock samples that showed successive degrees of leaching (L91–R3A and B) and oxidation

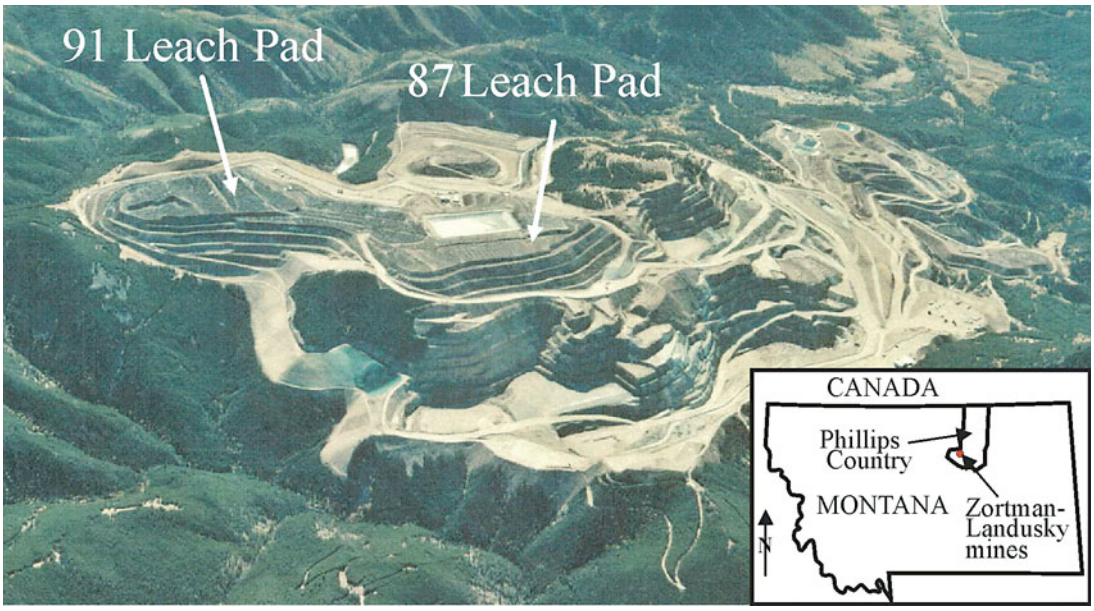

FIG. 1. An aerial view of the spent cyanide leach-pads at the Landusky–Zortman gold mines.

(L87–R6A, B and C). The degree of leaching was estimated from the intensity of a blue coloration on pyrite caused by a film of iron cyanide. The degree of oxidation was estimated visually from the development of a yellow or reddish ocher on pyrite. Grains with differing degrees of alteration were collected using a binocular microscope. If pyrite in the assemblage with the Al phase is shiny and yellow, we classified the Al mineral as weakly leached. If pyrite is black with a bluish film, the Al phase is considered to be strongly leached. Red and brown tints on pyrite indicated weathering of the Al minerals in association with the oxidation of pyrite.

Polished thin sections and individual grain-mounts were prepared for electron-microprobe analysis, without the use of water in order to preserve soluble minerals.

Samples of drainage water were collected in August 2002 from both the L91 and the L87 leach pads in the vicinity of the water-treatment plant. Dissolved oxygen (DO) and pH were measured in the field immediately after sampling, the precision of the pH measurements being ±0.08. Two liters of each sample were passed through 0.45 mm filters. Two 500 mL aliquots were acidified with HNO_3 to preserve the concentrations of dissolved metal, and the remainder left unacidified for anion analysis. The water samples were stored in an ice-filled cooler until analysis.

TABLE 1. SAMPLES REPRESENTING DIFFERENT STAGES OF ALTERATION OF SYENITE AND PROPORTIONS OF PHYLLOSILICATES IN THE < 2 μm FRACTION, AS DETERMINED BY XRD

Sample	Description*	Illite	Smectite	Kaolinite
	Unleached syenite			
R18	slightly hydrothermally altered, slightly weathered	Major	-	-
R6	slightly hydrothermally altered, slightly weathered	Major	-	Major
R15	slightly hydrothermally altered, moderately weathered	Minor	-	Major
R7	moderately hydrothermally altered, moderately weathered	Major	-	Major
	Heap-leached syenite			
L91-R3(A)	weakly leached, weakly oxidized	Major	Minor	Trace
L91-R3(B)	moderately leached, weakly oxidized	Major	Major	-
L87-R6(A)	strongly leached, weakly oxidized	Minor	Major	Trace
L87-R6(B)	strongly leached, moderately oxidized	Minor	Major	Minor
L87-R6(C)	strongly leached, strongly oxidized	Minor	Major	Major

* see the text for explanations.

Analytical techniques

Concentrations of cations in water samples were determined by Cantest Ltd., Vancouver, using inductively coupled plasma – mass spectrometry (ICP–MS), that of anions by ion chromatography, the level of alkalinity with an autotitrator, and that of nitrate using an auto-analyzer.

Solid phases were identified in polished thin sections using optical microscopy, where possible. Individual grains were mounted on aluminum stubs and examined for morphological features using a scanning electron

microscope (SEM, Stereoscan 120, Cambridge Instruments) and analyzed qualitatively with an X-ray energy-dispersion spectral analyzer (EDS). Feldspars grains were washed clean of clay particles in an ultrasonic disaggregator before mounting on an SEM stub for observation of surficial features.

Selected grains from polished grain-mounts and thin sections were analyzed with a CAMECA–SX100 electron microprobe, operated at an acceleration potential of 15 kV and a beam current of 15 nA, except 8 kV and 20 nA for oxygen. A beam of 1 μm diameter was used for fine-grained clays, 5 μm for feldspars and micas, and 20 μm for amorphous materials. K-feldspar (K), diopside (Ca, Si,O), andalusite (Al), albite (Na), olivine (Fe, Mg), spinel (Ti, Zn) and artificial alloys (Cu, S) were used as standards. The raw data were corrected by the PAP correction procedure (Pouchou & Pichoir 1984). Detection limits for different components varied from 0.01 to 0.05 wt.%, and analytical precision was approximately 2% for most major elements, and 10% for minor elements. The possibility of induced K and Na migration from phyllosilicates under the electron beam was examined by collecting data over intervals of 5 s for mica and 2 s for clays over a total period of 30 s. The diameter of the beam was also varied from 1 to 5 μm to estimate the effect of beam size on element migration.

Phyllosilicates were identified by XRD using oriented mounts. Rock samples were crushed to <5 mm and sieved to separate the <63 μm fraction. Clay aggregates were scratched from the surfaces of leached samples of syenite and also picked out of etch pits in feldspar grains. These clay samples were ground in an agate mortar for 5 minutes. Clumps of fine particles were disaggregated in distilled water in an ultrasonic bath for 30 minutes. The >2 μm size fraction was deposited from the suspension by centrifuging at 2000 rpm for 2–3 minutes, and then the suspension of <2 μm was transferred to a Millipore® filtration system to prepare oriented mounts (Moore & Reynolds 1997). Three separate mounts were prepared for each sample, which included (1) air-dried at room temperature, (2) glycolated for 24 h, and (3) heated at 550°C for 1 h. XRD traces were obtained using a Philips PW 1729 diffractometer operated under Ni-filtered Cu*K*α radiation generated at 40 kV and 40 mA, using a 0.5° beam slit. Scans were recorded with steps of 0.05° at a rate of 1.5° 2θ per minute over the range 3–65° 2θ.

The relative proportions of phyllosilicates were determined from the XRD data according to the scheme of Johns *et al.* (1954) with one exception. Johns *et al.* (1954) used a ratio of 4:1 for the intensity of the 17 Å peak of glycolated smectite to the 10 Å peak of collapsed smectite. However, we found this ratio to be 6.3 ± 0.5. This difference in peak ratios may be due to either a thinner film of clay in the mount, or to a higher intensity of the X-ray beam than used by Johns *et al.* (1954). The percentage of expandable component was calculated from the ratio of the areas of the 10 Å peak in the glycolated *versus* the trace of the heated sample, which is proportional to the quantity of illite and illite + smectite. The area ratio of the 7 Å to 10 Å peak in the glycolated material, which reflects the proportion of kaolinite and chlorite to illite, was taken as equal to one because of the low crystallinity index of the Landusky kaolinite (Schultz 1958, 1964). This semiquantitative scheme was suitable to distinguish the major, minor and trace amounts of phyllosilicates in each sample.

Several <2 μm sample fractions that seemed, according to XRD results, to contain only smectite, were analyzed by inductively coupled plasma – optical emission spectroscopy (ICP–OES) for alkali content to verify the electron-microprobe data. The powdered samples were removed from the XRD mount, weighed into a 50 mL centrifuge tubes, dried at 110°C overnight, and reweighed to calculate the loss on heating. They were digested in 8.5 mL HNO_3 and 1.5 mL HF and heated in a microwave oven (model MDS–210, CEM Co.) at 95°C for 60 min. After cooling to room temperature, 20 mL of distilled water was added to the samples, and they were reheated at 80°C for 60 min. The digested samples were cooled and analyzed using a Varian Liberty 200 spectrometer referenced to ICP standard solutions (SCP Science).

RESULTS

In Table 1, we summarize the results obtained on the rock samples in terms of their apparent degree of alteration and weathering through hydrothermal alteration, natural weathering, cyanide leaching and sulfide oxidation.

TABLE 2. RESULTS OF ELECTRON-MICROPROBE ANALYSES AND CALCULATED FORMULAE OF FELDSPARS FROM UNLEACHED SYENITE

	K-feldspar, *n* = 6		Albite, *n* = 9	
	Ave.	St. dev.	Ave.	St. dev.
SiO_2 wt%	64.7	(0.23)	68.6	(0.75)
Al_2O_3	18.4	(0.14)	19.6	(0.34)
CaO	<0.03	(-)	0.13	(0.12)
Na_2O	0.81	(0.35)	11.7	(0.26)
K_2O	15.5	(0.56)	0.14	(0.09)
Total	99.4	(0.31)	100.1	(1.15)
Si	3.09	(0.018)	2.99	(0.008)
Al	1.03	(0.008)	1.01	(0.010)
Si + Al	4.12	(0.026)	4.00	(0.018)
Ca	-	(-)	0.01	(0.005)
Na	0.07	(0.032)	0.99	(0.015)
K	0.94	(0.035)	0.01	(0.005)
Σ alkalis	1.01	(0.067)	1.00	(0.020)

The number of cations is calculated on the basis of 8 atoms of oxygen. Samples R18, R15, and R7. *n*: number of grains analyzed.

The feldspars

The feldspars are the main Al-containing minerals in the unaltered samples of syenite; their composition is given in Table 2. Phenocrysts (5–15 mm in length) of orthoclase and rare microcline in a groundmass of quartz, plagioclase and K-feldspar constitute up to 75% of the syenite. The plagioclase content is approximately half that of K-feldspar, with plagioclase phenocrysts, 2–3 mm in length, being predominantly sodic (Table 2).

The phenocrysts in hydrothermally altered, slightly weathered syenite show features of secondary growths (Figs. 2a, b), and cavities on their surface that contain illite. In leach-pad samples affected by alkaline cyanide solutions, orthoclase and microcline phenocrysts show elongate etch-pits (Fig. 2c). Such pits are common features of feldspar dissolution (Berner & Holdren 1977), forming at dislocations along twin boundaries or marking edge dislocations along curved low-angle boundaries (Berner & Holdren 1979). The K-feldspar grain shown in Figure 2d has elongate dissolution-pits parallel to (010), which have apparently formed along cleavages. Orthoclase grains in the cyanide-leached, strongly oxidized syenite have similar surface features to those in the weakly oxidized, cyanide-leached rocks.

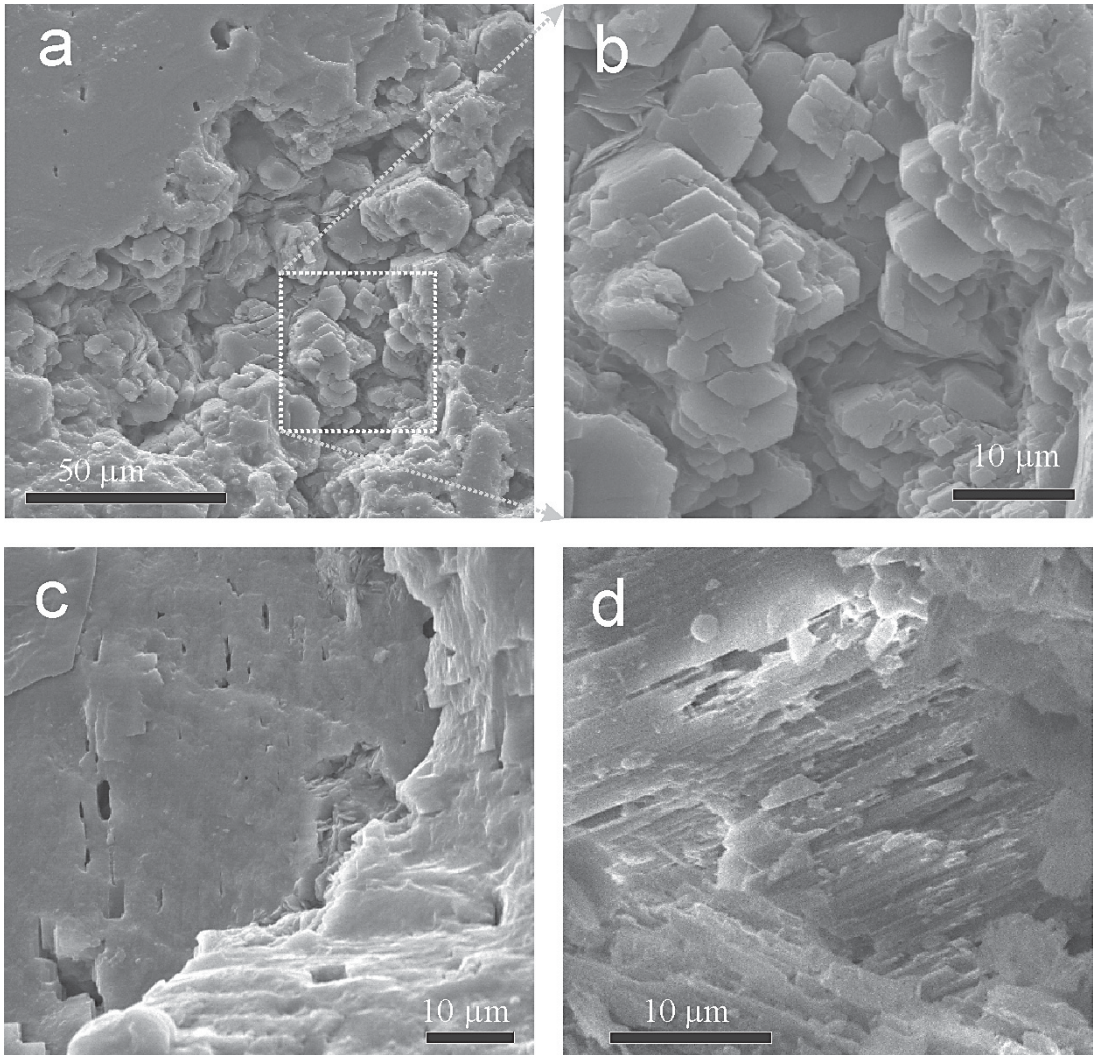

FIG. 2. SEM images of feldspar grains: (a, b) secondary growth of K-feldspar on the surface of slightly hydrothermally altered and moderately weathered orthoclase. Etch pits on the surface of (c) moderately and (d) strongly leached orthoclase.

Illite

Illite is present in all the samples and is the dominant phyllosilicate in the unleached and slightly weathered syenite (Table 1). The gold mineralization at Landusky was associated with illite formation in altered intrusive rocks (Wilson & Kyser 1988). Three types of illite were distinguished here on the basis of optical properties and morphology. Type I consists of 40–150 μm colorless crystals forming rosettes (Fig. 3a) in cavities in orthoclase (Fig. 3b), probably by utilizing elements from the dissolution of feldspar. Type II is a white illite, which forms fine aggregates over the K-feldspar surfaces (Fig. 3c). Light brown Type-III illite, the most abundant in all rocks sampled, is associated with unaltered pyrite. A hydrothermal origin for Type-III illite can be inferred, because pyrite associated with this illite is unaltered in most cases. Grains of type-III illite are richer in Fe in comparison with two first types (Table 3). Iron apparently substitutes for Al, because Fe concentration is inversely proportional to Al (Fig. 4). This substitution is very common in the layer of octahedra because of the similar ionic size of Al^{3+} and Fe^{3+} (Newman & Brown 1987).

All three types of illite contain a lower proportion of alkali cations than typical illite. Hower & Mowatt (1966) found that typical illite containing <10% smectite interlayers has about 1.5 (K + Na) per 44 negative charges. The low content of alkali ions in our samples of illite may be due to (a) the presence of smectite, (b) a high content of H_2O, or (c) the migration of alkali cations under the electron beam (Autefage 1980). The presence of mixed-layer phyllosilicates was investigated by using the position, shape and intensity of the (001) reflection of illite when glycolated (Moore & Reynolds 1997). Where illite contains >10 % smectite, the (001) reflection should be observed at >9.01° 2θ. However, the (001) reflections in our samples did not reach this value, varying from 8.86 to 8.92° 2θ (Figs. 5a–d). The peaks are symmetrical, without the shoulders that would be found on the high-angle side of the peak if interlayered illite–smectite were present (Figs. 5c, d). Also, differences in peak intensities did not exceed 6% between air-dried and glycolated states (*i.e.,* within the error of the measurements). Therefore, mixed-layer illite–smectite does not appear to be present, and illite contains <10% of expandable layers.

A high content of H_2O could explain the low content of the alkalis. Loucks (1991) reported illite containing <0.2 (K + Na + Ca) atoms per formula unit (*apfu*) and suggested that H_2O and H_3O^+ could be present as interlayer molecules in the alkali-poor mica, contrary to the model of Hower & Mowatt (1966) for "typical" illite.

The possible migration of alkali cations under the electron beam was tested by measuring the number of counts for alkali metals over varying periods of time. The counts for K decreased over 30 s by 2.5% of the counts that accumulated during the first 5 s, with a 5 μm beam size, and by 10% with a 1 μm beam (Fig. 6a). As the data for illite were obtained with a 5 μm beam, K migration was considered to be insignificant. Sodium counts for illite varied randomly with time owing to the low intensity of the peak, which is close to the background. Because the concentration of Na is low, migration of Na during analysis would not have a significant effect on the total alkali content.

Smectite

Smectite was found only in the post-leach samples (L91–R3 and L87–R6 in Table 1). Rims were observed around illite in the cyanide-leached ore. These rims are depleted in K, but have similar levels of Al, Fe and Si (Fig. 7), indicating replacement of illite by the K-analogue of smectite. In some samples, smectite forms platy grains with irregular shapes and is associated with kaolinite (Fig. 8a). XRD patterns of smectite are characterized by a broad (001) reflection with a

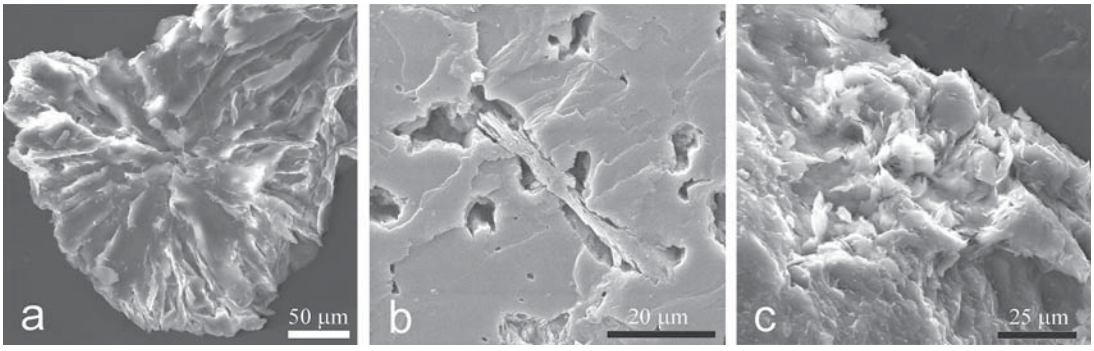

FIG. 3. SEM images of illite: Type I (a) forming a rosette, and (b) filling a cavity in hydrothermally altered orthoclase. (c) Leaf-like crystals of Type II on the surface of K-feldspar.

maximum close to 7.35° 2θ, which is common for K- and Na-exchanged smectites (Brown & Brindley 1980). The presence of kaolinite or illite interlayers in a smectite matrix could be detected from the (002) glycolated reflection, which appears between 10.30° and 10.33° 2θ in our samples (Figs. 5d–f). For detectable smectite–kaolinite interlayering (>10% of kaolinite), the peak position should be at >10.46° 2θ, and if over 10% illite is mixed with smectite, the (001–002) reflection would be at <10.31° 2θ (Moore & Reynolds 1997).

The formula of the smectite was initially calculated to be $(Al_{3.57}\ Fe^{3+}_{0.35}\ Mg_{0.28})(Al_{0.65}\ Si_{7.35})\ (K_{0.14}\ Ca_{0.08}\ Na_{0.03})O_{22}(OH_4)\bullet nH_2O$ from the average result of the electron-microprobe analyses (Table 4). This composition is closer to a K-exchanged analogue of beidellite than to montmorillonite because of the negative layer-charge from Al^{3+} in tetrahedral sites, although the number of interlayer cations per formula unit is lower than usually observed in beidellite (Newman & Brown 1987).

The decrease in electron-microprobe counts for K by 41% of the initial value, during the collection time of 30 s with a 1 μm beam (Fig. 6b), indicates that the measured concentration of K is affected significantly by the loss of K. It was not possible to use a larger beam (as was done for illite) to analyze only smectite in inseparable smectite–kaolinite or smectite–illite aggregates. Therefore, the concentration of alkalis was measured by ICP–OES in bulk-clay fractions of samples L–87–R6 (A) and L–87–R6, in which smectite dominates (Table 1). Higher contents of K (1.73 ± 0.29 wt.% K_2O) and Na (0.34 ± 0.04 wt.% Na_2O) were detected by ICP–OES than with the electron microprobe (Table 4), but the concentration of Ca (0.49 ± 0.04 wt.% CaO) was found to be the same. These values were recalculated to take into account the weight loss on heating, and used for formula calculations. The K-dominant analogue of beidellite is assumed to be the dominant phase containing significant amounts of alkali metals, because the proportion of illite is low (Table 1). The formula was recalculated by replacing the electron-microprobe data for K_2O, Na_2O, and CaO (Table 4) by ICP–OES values. The resulting formula, $(Al_{3.52}\ Fe^{3+}_{0.35}\ Mg_{0.27})(Al_{0.69}\ Si_{7.31})(K_{0.30}\ Na_{0.09}\ Ca_{0.07})O_{22}(OH_4)\bullet nH_2O$, contains twice as many interlayer cations and is closer to naturally occurring beidellite (Newman & Brown 1987).

TABLE 3. RESULTS OF ELECTRON-MICROPROBE ANALYSES AND CALCULATED FORMULAE FOR VARIETIES OF ILLITE FROM UNLEACHED SYENITE

	Type I, Colorless $n = 20$		Type II, White $n = 12$		Type III, Brown $n = 17$	
	Ave.	St. dev.	Ave.	St. dev.	Ave.	St. dev.
SiO_2 wt%	50.21	(1.22)	49.44	(1.65)	49.81	(1.46)
Al_2O_3	29.56	(1.04)	29.36	(0.88)	26.85	(1.81)
TiO_2	0.063	(0.033)	0.057	(0.034)	0.061	(0.030)
Fe_2O_3	3.17	(0.38)	3.27	(0.40)	4.44	(0.92)
MnO	0.012	(0.019)	0.008	(0.010)	0.016	(0.017)
MgO	1.67	(0.24)	1.56	(0.29)	1.55	(0.26)
CaO	0.22	(0.08)	0.20	(0.06)	0.23	(0.10)
Na_2O	0.067	(0.012)	0.070	(0.014)	0.070	(0.018)
K_2O	7.01	(0.95)	6.58	(1.18)	6.01	(1.27)
F	0.40	(0.05)	0.36	(0.05)	0.38	(0.05)
Total	92.38	(4.02)	90.91	(4.57)	89.42	(5.94)
Si *apfu*	6.75	(0.06)	6.74	(0.04)	6.91	(0.14)
Al	1.25	(0.06)	1.26	(0.04)	1.09	(0.14)
Σ tetrahedral	8.00	(-)	8.00	(-)	8.00	(-)
Al	3.44	(0.09)	3.46	(0.10)	3.29	(0.18)
Ti	0.007	(0.003)	0.007	(0.003)	0.006	(0.003)
Fe^{3+}	0.32	(0.04)	0.34	(0.04)	0.46	(0.10)
Mn	0.001	(0.002)	0.002	(0.001)	0.002	(0.002)
Mg	0.33	(0.05)	0.31	(0.05)	0.32	(0.05)
Σ octahedral	4.10	(0.18)	4.12	(0.20)	4.09	(0.34)
Na	0.02	(0.003)	0.02	(0.004)	0.02	(0.005)
K	1.20	(0.16)	1.14	(0.18)	1.06	(0.21)
Ca	0.03	(0.01)	0.03	(0.01)	0.03	(0.02)
Σ interlayer	1.25	(0.17)	1.19	(0.20)	1.12	(0.22)

The number of atoms is calculated on the basis of $O_{50}(OH,F)_4$. *n*: number of analyses made. Samples R6, R18, and R7.

Minerals of the kaolinite group

Kaolinite was detected in naturally weathered rocks (Figs. 5b,c), cyanide-leached and post-leach oxidized rocks (Figs. 5e, f). It usually forms irregular platy aggregates, and occasionally hexagonal crystals (Figs. 8a, b). A crystallinity index of 2 was determined from the ratio of the 7 Å peak area to height in the glycolated equivalent (Schultz 1958, 1964). The dominant polytype of the kaolinite group (kaolinite, dickite or nacrite) could not be identified because of the low crystallinity.

Peaks at 12.20–12.35° 2θ relate to the (001) reflection of kaolinite containing less than 10% smectite (Moore & Reynolds 1997). Changes in shape, area, and height of the (001) reflection at ~12.3° 2θ after glycolation (Figs. 5c, f) could be due to the presence of small amounts of smectite interlayers in the kaolinite matrix. The calculated formula shows higher proportions of silicon and alkalis per formula unit (Table 4) than published formulae (Newman & Brown 1987), which may be due to kaolinite–smectite interlayering.

Other phyllosilicates

A residual peak at ~12.3° 2θ in two samples after heat treatment (*e.g.*, Fig. 5e) may be due to chlorite, as heating at 550°C for 1 hour would destroy the kaolinite structure (Johns *et al.* 1954). However, since the chlorite reflections at ~6.3° and ~3.5° 2θ were not observed in the air-dry state, the presence of chlorite remains uncertain.

The SEM image of a cyanide-leached and oxidized sample L87–R6(C) shows fibrous crystals containing Si, Al and Fe covering smectite (Fig. 8c), suggesting the presence of halloysite (Henning & Störr 1986). However, the main reflection of halloysite at ~10° 2θ

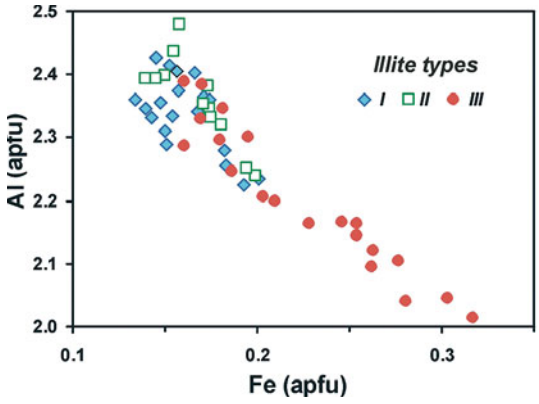

FIG. 4. A plot of the Fe *versus* Al content of illite, in atoms per formula unit (*apfu*).

was not observed in the air-dried XRD traces, possibly owing to its low concentration.

Phases precipitated from drainage solutions

The precipitate sample (F3) was found by ICP–OES analysis to contain 66.38% Al_2O_3, 20.05% SiO_2, 6.46% SO_4, 2.96% CaO, 0.59 CuO, 1.96% FeO and 1.58% Na_2O. This precipitate was subdivided into three separate portions based on color (white, blue and brown). An XRD trace of the white portion showed it to be almost amorphous without an expandable component, as it gave a high background and only weak, broad reflections with 2θ values of 7.5–9.0°, 16.5–17.5° and 25–27°. Back-scattered electron images (SEM) show zonation in the white portion (Fig. 9a). Zones contain

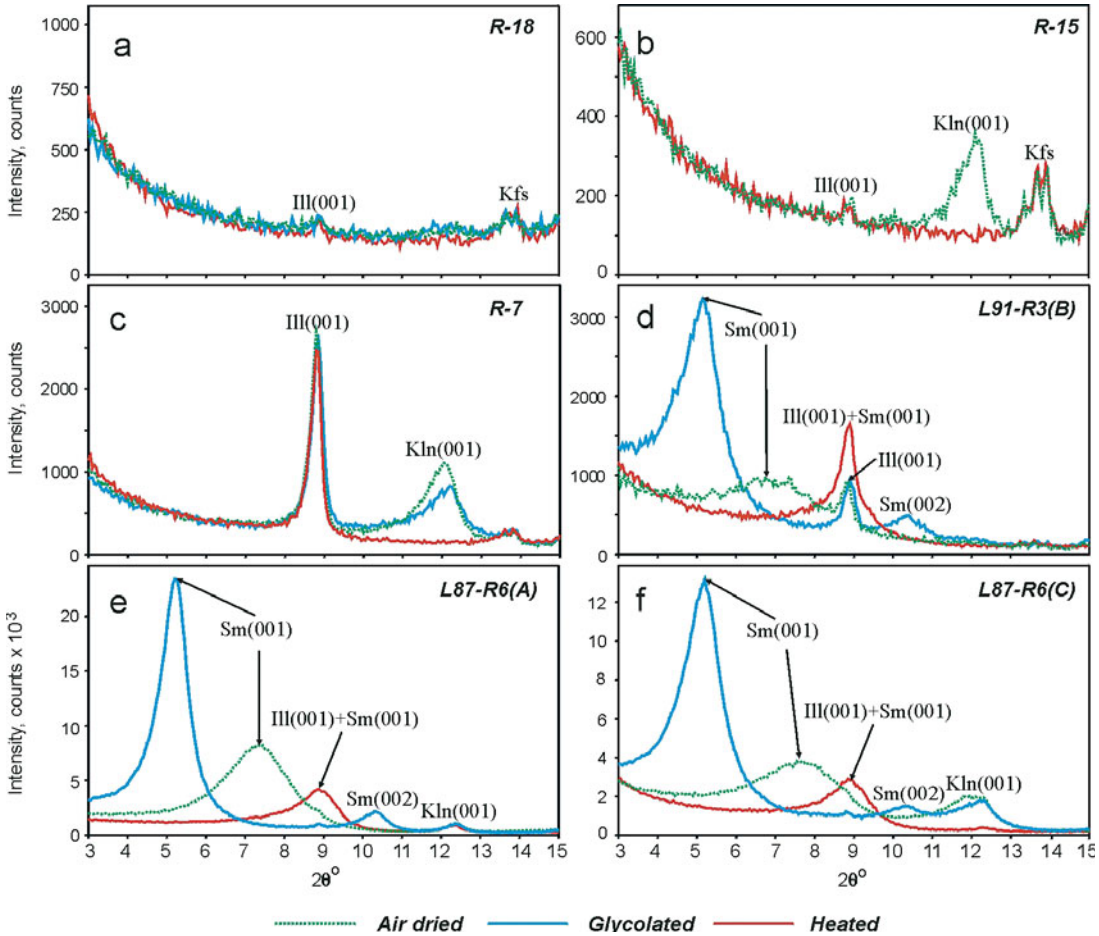

FIG. 5. The low-angle regions of XRD patterns of the <2 μm fraction of phyllosilicates after drying in air, after glycolation and after heat treatment: (a) slightly hydrothermally altered, slightly weathered, (b) slightly hydrothermally altered, moderately weathered, (c) moderately hydrothermally altered, moderately weathered, (d) moderately leached, weakly oxidized, (e) strongly leached, weakly oxidized, (f) strongly leached, strongly oxidized. Ill: illite, Kfs: K-feldspar, Kln: kaolinite, and Sm: smectite.

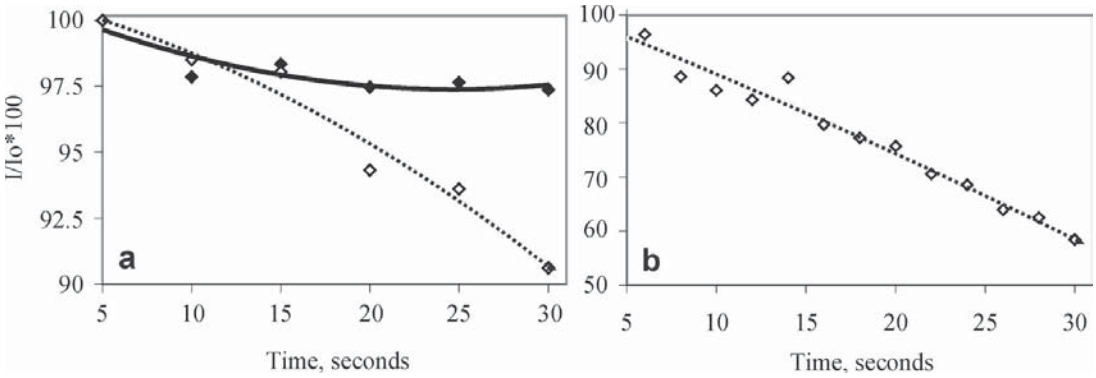

FIG. 6. The relative intensity of the K peak during electron-microprobe analysis of (a) illite and (b) smectite. Relative intensity (I/I_o*100) is the measured intensity (I) expressed as a percentage of the initial counts (I_o) collected during the first five seconds. Open diamonds represent the intensities with a 1 μm beam (dashed trend line), and the solid diamonds, with a 5 μm beam (black trend line). The trend lines were constrained by a second-order polynomial.

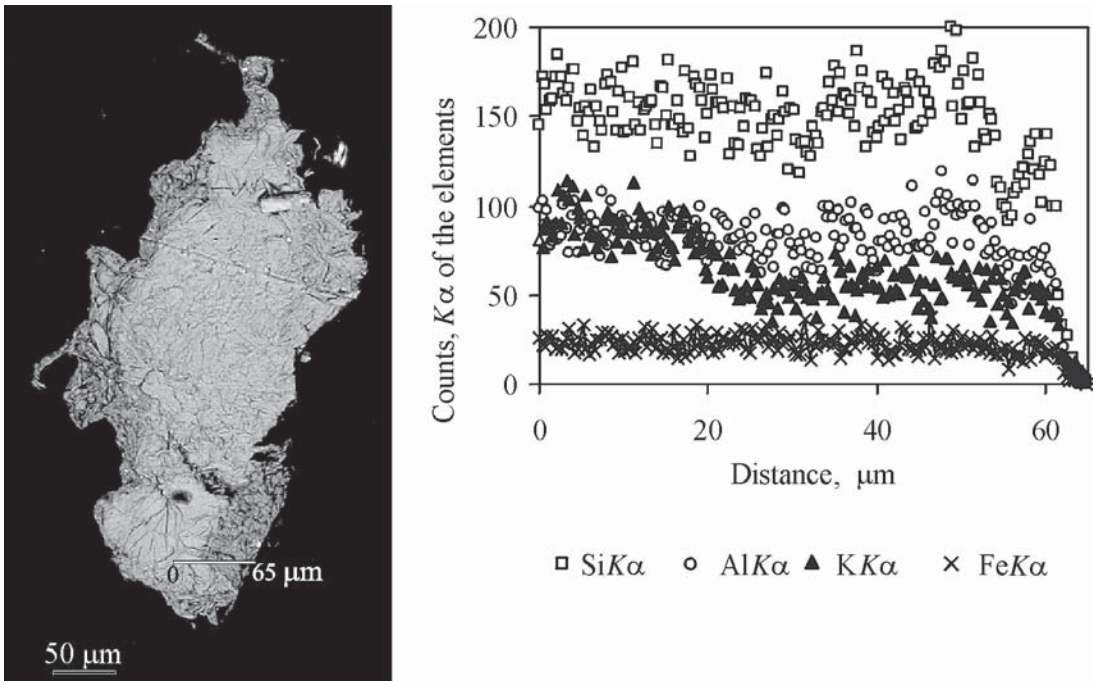

FIG. 7. Back-scattered electron image (SEM) showing a rim around an illite grain from sample L91–R3(B) and *K*α counts of Al, Si, K and Fe in a profile from the core through the rim.

similar proportions of Al, Si, Ca, S, Fe, and Na, but the concentration of H_2O could be different, resulting in the zoning appearing under SEM. Electron-microprobe analyses of the brightest zones (Fig. 9a) gave 40.1 (±7.6) wt.% O, 21.1 (± 3.2) wt.% Al, 4.2 (± 0.6) wt.% Si and 0.5–1 wt.% Ca, S, Fe, and Na. The average O:Al atom ratio, 1.90, is close to that of the aluminum oxyhydroxides, such as böhmite and diaspore.

Native copper and cuprite were identified by XRD in the blue portion of the precipitate. There were

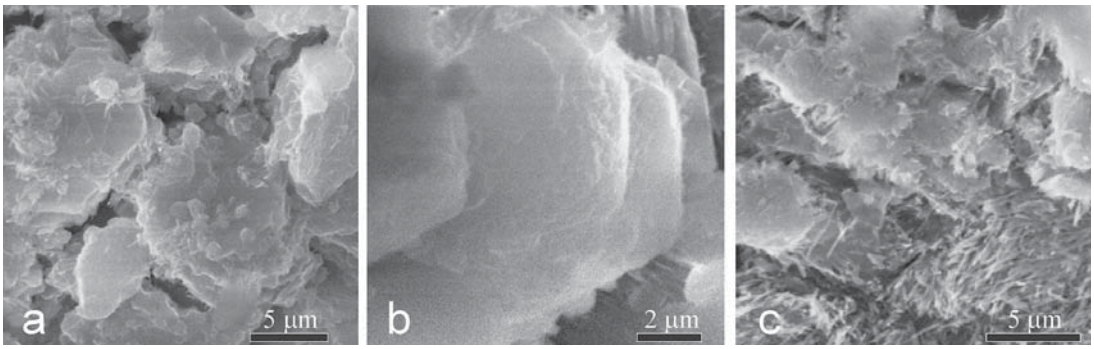

FIG. 8. SEM images of clay minerals: (a) an aggregate of smectite and kaolinite, (b) kaolinite crystals, (c) fabric halloysite.

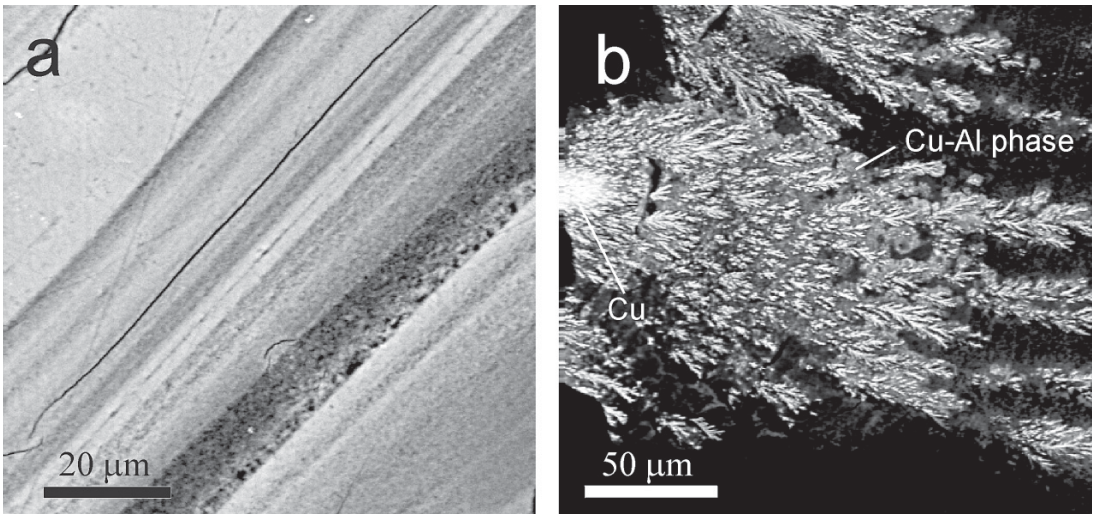

FIG. 9. Back-scattered electron images (SEM) of the precipitate from the pipe, sample F3: (a) zoned precipitate of Al hydroxides, (b) dendrites of Cu surrounded by hydroxides of Cu–Al phase.

also weak peaks with *d*-values of 10.64, 5.17, 2.45, and 2.24 Å that could be due to copper hydroxide and hydrowoodwardite $Cu_{1-x}Al_x(OH)_2(SO_4)_{x/2}(H_2O)_n$ (Witzke 1999). Copper dendrites surrounded by fine grains containing Cu and Al were observed by SEM in the precipitate (Fig. 9b). The brown portion shows two weak reflections at 3.37 and 1.80° 2θ. The brown substance consists of Al–Si phases similar to the white portion, but covered by a film of Fe oxyhydroxides, as indicated by SEM–EDS analysis.

Water analyses and modeling

Oxidation of pyrite in the leached material is indicated by the presence of corroded surfaces of grains (Fig. 10a), and by the high concentrations of sulfate in the drainage water (Table 5). The localized acidity caused by pyrite oxidation may have contributed to the dissolution of adjacent illite (Fig. 10b) and resulted in a redistribution of Al. The increase in acidity is indicated by the higher pH of the water in 2000 (7.06) than in 2001 and 2002 (6.40 and 6.54). The concentration of Al attained a maximum value of 24.9 mg/L in June 2001 at the lowest value of pH. The composition of the water draining L91 is similar to that from L87, except for higher concentrations of Al and Fe (Table 5). From 2000 to 2001, an increase in the pH of the L91 drainage, from 5.67 to 6.55, due to the addition of lime to the pile, caused a decrease in the concentration of Al. By 2002, pH had again dropped (pH = 4.31), and the concentra-

tion of Al increased to 86.8 mg/L. There is a significant negative correlation between pH and Al concentration (r^2 = –0.95) for the six samples presented in Table 5.

Calculations using WATEQ4f (Ball *et al*. 1987) indicate that in 2002, about 90% of Al in L87 was bound in the hydroxide complexes $Al(OH)_4^-$ and $Al(OH)_2^+$, whereas in L91, the sulfate complexes $AlSO_4^+$ and $Al(SO_4)_2^-$ dominated. Saturation indices (SI) close to zero indicate the presence of phases controlling the concentration of Al and Si by precipitation and disso-

TABLE 4. RESULTS OF ELECTRON-MICROPROBE ANALYSES AND CALCULATED FORMULAE OF SMECTITE AND KAOLINITE

	Smectite, *n* = 7		Kaolinite, *n* = 5	
	Ave.	St. dev.	Ave.	St. dev.
SiO_2 wt%	54.26	(1.13)	48.16	(0.22)
Al_2O_3	26.52	(2.46)	37.68	(0.84)
Fe_2O_3	3.46	(0.73)	0.62	(0.16)
MgO	1.37	(0.22)	0.12	(0.07)
CaO	0.53	(0.14)	0.08	(0.02)
Na_2O	0.10	(0.06)	0.02	(0.01)
K_2O	0.79	(0.26)	0.27	(0.24)
Total	87.04	(5.01)	86.95	(1.56)
Si *apfu*	7.35	(0.16)	4.11	(0.04)
Al	0.65	(0.16)	-	-
Σ tetrahedral	8.00	-	4.11	(0.04)
Al	3.57	(0.17)	3.79	(0.06)
Fe^{3+}	0.35	(0.08)	0.04	(0.01)
Mg	0.28	(0.05)	0.02	(0.01)
Σ octahedral	4.20	(0.30)	3.85	(0.08)
Na	0.03	(0.05)	0.004	(0.002)
K	0.14	(0.02)	0.03	(0.03)
Ca	0.08	(0.02)	0.01	(0.001)
Σ interlayer	0.25	(0.09)	0.04	(0.03)

Samples: R91-R3(B), R87-R6(B-C); *n*: number of analyses. The number of cations in smectite is calculated on the basis of $O_{20}(OH)_4$; that in kaolinite, on the basis of $O_{10}(OH)_8$.

TABLE 5. COMPOSITION OF THE WATER DRAINING LEACH PADS L87 AND L91

	L87			L91		
Date	A.2000*	6/2001*	8/2002	A.2000*	6/2001*	8/2002
pH	7.06	6.40	6.54	5.67	6.55	4.31
Conductivity§	-	-	8780	-	-	7880
HCO_3^- mg/L	-	-	83	-	-	-
F^-	-	-	<1	-	-	4
Cl^-	-	-	104	-	-	106
NO_3^-	250	-	227	282	-	220
SO_4^{2-}	4440	4460	4540	4170	4140	4650
Al	0.1	24.9	0.68	23.5	13.4	86.8
As	-	-	0.014	-	-	0.038
Ba	-	-	0.017	-	-	0.015
Ca	460	460	313	499	547	593
Co	-	-	1.85	-	-	1.41
Cu	-	-	0.24	-	-	0.98
Fe	0.8	1.0	0.4	5.0	4.82	13.6
K			18.8	-	-	15.2
Mg	80	179	74.9	68.4	78.4	129
Mn	14.9	43.6	12.6	16.0	15.5	36
Na	-	-	2030	-	-	1390
Ni	0.4	1.07	0.3	0.46	0.29	1.25
PO_4^{3-}	-	-	0.75	-	-	0.57
Se	0.85	0.65	0.83	1.2	1.3	1.04
SiO_2	-	-	22.3	-	-	54.2
Sr	-	-	1.4	-	-	0.64
Tl	-	-	<0.001	-	-	0.079
Zn	1.25	6.33	1.75	2.83	2.31	8.29

A.2000: average data for 2000. -: not analyzed. § Conductivity is reported in μS/cm.
* Data from Applied Biosciences Corporation (2001).

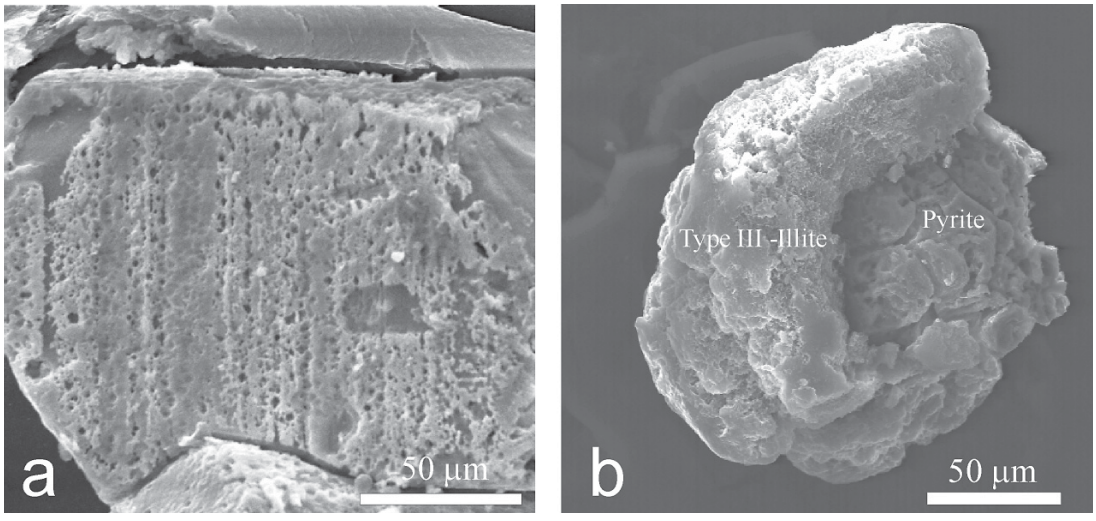

FIG. 10. Back-scattered electron images (SEM) showing (a) a corroded surface of a pyrite grain, and (b) pyrite surrounded by Type-III illite.

lution. According to this criterion, Si concentration in drainage L87 and L91 could be controlled by the precipitation of amorphous silica (SI = –0.4 and 0) or "chalcedony" (0.1 and 0.5). In the case of aluminum, the water from L87 was close to saturation with respect to only allophane (SI = 0.5) and amorphous $Al(OH)_3$ (SI = 0.5), whereas for L91, the saturation indices of basaluminite, böhmite, and gibbsite also were close to zero.

The stability of the major secondary Al-rich phases, kaolinite and the K-dominant analogue of beidellite, was calculated using the Geochemist's Workbench (Bethke 2002) for various values of pH. The effect of pH on the relative stability of these minerals can be expressed by reaction (1).

$$(Al_2)(Al_{0.33}Si_{3.67})(K_{0.33})O_{10}(OH_2)\bullet nH_2O + 0.33\ H^+ = 1.165\ Al_2Si_2O_5(OH)_4 + 1.34\ SiO_{2(aq)} + 0.33\ K^+ + (n - 1.165)\ H_2O \quad (1)$$

This shows the K-dominant analogue of beidellite (simplified formula) to be more stable in basic conditions than kaolinite. If the activities of H_2O and solid phases are assumed to be 1, the equilibrium constant for the reaction is

$$\log K = 1.34 \log a\ [SiO_{2(aq)}] + 0.33\ pH + 0.33 \log a[K^+] \quad (2).$$

The pH of the boundary between the two minerals can be calculated if the other variables in equation (2) are known. The reaction constant was found to be –2.608 at 25°C (Geochemist's Workbench database). The average composition of the L87 and L91 water (Table 5) were used for the activities of $SiO_{2(aq)}$ and K^+. Substitution into equation (2) gives a pH of 8.44 for the equilibrium boundary between kaolinite and the K-dominant analogue of beidellite in the presence of the solution. However, the boundary shifts significantly if the activities of elements vary, particularly that of dissolved SiO_2. If log $a[SiO_{2(aq)}]$ is changed from –3.420 to –3.044, as in samples L–87 and L–91, respectively, the boundary will move from pH 7.82 to 9.38.

These calculations show that the K-dominant analogue of beidellite could be formed under the alkaline conditions of the cyanide leaching process (pH ≈ 10). After rinsing and with subsequent increases in acidity, the formation of kaolinite would be expected.

Discussion

Understanding the history of both natural and anthropogenic processes is key to understanding the mineralogical changes and water-quality evolution that have developed in the Landusky leach-pads. The processes of interest include: hydrothermal alteration, pre-mining weathering, cyanide leaching, post-mining treatment and weathering.

The hydrothermal alteration of syenite resulted in a partial replacement of feldspars by illite. This was the first natural step in the transformation of aluminosilicates. During the next step, pre-mining weathering of illite and feldspars resulted in the formation of kaolinite. Wilson & Kyser (1988) described montmorillonite formation from weathered syenites in the Landusky host-rock but, in this study, smectite was found only in samples leached by cyanide (Table 1).

During mining, the surface area of the rock was increased substantially, thereby increasing the susceptibility of the rocks to additional weathering. The effects of cyanide leaching at pH ≈ 10 caused the dissolution of feldspars and illite with a significant increase in smectite concentration (Table 1). Thermodynamic considerations show the K-dominant analogue of beidellite (smectite) to be stable under these alkaline conditions.

Once leaching ceased, at the stage of rinsing and post-mining weathering, thermodynamic calculations indicate that increased acidity resulted in the dissolution of the smectite. Similar observations of smectite dissolution in acidic mine-water have been reported by others (*e.g.*, Galán *et al.* 1999). A correlation between the state of weathering of the post-leached samples and the proportion of kaolinite in the clay fraction (Table 1) shows that with decreasing pH, kaolinite was formed after smectite. The increasing acidity eventually resulted in the dissolution of kaolinite and a rise in Al concentration in the drainage water.

The concentration of Al in acidic mine-drainage waters is strongly dependent on pH owing to hydrolysis, resulting in the formation of Al hydroxide and hydroxysulfate precipitates from solution (Nordstrom 1982). Geochemical modeling of the Landusky drainage water shows that the concentrations of Al can be controlled by the precipitation of Al hydroxide. The presence of amorphous Al hydroxide in the precipitate from the pipe supports the modeling results. Although the Al:O ratio of the precipitate has a stoichiometry close to that of böhmite, there were no böhmite peaks in the XRD pattern. Böhmite would not be expected to precipitate directly from solution under conditions of weathering, but would rather crystallize from Al hydroxides by dehydration.

Conclusions

The hydrothermal alteration of syenite, during the deposition of the gold-bearing pyrite, caused alkali feldspar and plagioclase to be partially converted to illite. Extraction of gold with a NaCN solution at pH ≈ 10 caused further dissolution of the feldspars, and illite grains were altered, becoming laced with a K-dominant analogue of beidellite. Post-mining rinsing of the heaps and sulfide oxidation due to atmospheric weathering of the spent ore resulted in increasing acidity. The smectite became unstable as the pH dropped and formed kaolinite as an intermediate product. This kaolinite, as

well as other aluminosilicate minerals, dissolved when acidity continually increased, resulting in the high concentrations of Al in the drainage water.

The mineralogical and geochemical evolution of the spent ore from the Landusky leach-pads have dictated changes in the water-management system. In this study, we show the necessity of detailed mineralogical and geochemical characterization of the mine waste and the utilization of flexible, and adaptable water-treatment systems, especially in cases with extreme shifts in pH.

Acknowledgements

We thank Madeleine Corriveau for laboratory and field assistance, Ron Chapman for help with the electron microprobe, and Sergio Mejia for help with the SEM. Funding was provided by the Natural Sciences and Engineering Research Council of Canada, University of Manitoba Research and Development Fund, and the Queen's University Advisory Research Committee. Data and field assistance were provided by the Montana Department of Environmental Quality, the U.S. Bureau of Land Management, and Spectrum Engineering. Drs. Dogan Paktunc, Alan Turnock, two anonymous reviewers and Robert F. Martin provided helpful comments on this manuscript.

References

Applied Biosciences Corporation (2001): Zortman–Landusky water biotreatment system update: water chemistry changes at the Landusky 87 pad biotreatment site. Unpubl. Rep., Salt Lake City, Utah.

Autefage, F. (1980): Variations de la teneur en sodium et en potassium dans des minéraux au cours de leur analyse à la microsonde électronique. *Bull. Minéral.* **103**, 48-53.

Ball, J.W., Nordstrom, D.K. & Zachmann, D.W. (1987): WATEQ4F – a personal computer FORTRAN translation of the geochemical model WATEQ2 with revised data base. *U.S. Geol. Surv., Open-File Rep.* **87–50**.

Berner, R.A. & Holdren, G.R.J. (1977): Mechanism of feldspar weathering: some observational evidence. *Geology* **5**, 369-372.

_____ & _____ (1979): Mechanism of feldspar weathering. II. Observations of feldspars from soils. *Geochim. Cosmochim. Acta* **43**, 1173-1186.

Bethke, C.M. (2002): *Geochemist's Workbench. A Users Guide to Rxn, Act2, Tact, React, and Gtplot*. University of Illinois, Urbana, Illinois.

Blowes, D.W. & Jambor, J.L. (1990): The pore-water geochemistry and the mineralogy of the vadose zone of sulfide tailings, Waite Amulet, Quebec, Canada. *Appl. Geochem.* **5**, 327-346.

_____ & Ptacek, C.J. (1994): Acid-neutralization mechanisms in inactive mine tailings. *In* Environmental Geochemistry of Sulfide Mine Waste (J.L. Jambor & D.W. Blowes, eds.). *Mineral. Assoc. Can., Short Course Vol.* **22**, 271-292.

_____, Reardon, E.J., Jambor, J.L. & Cherry, J.A. (1991): The formation and potential importance of cemented layers in inactive sulfide mine tailings. *Geochim. Cosmochim. Acta* **55**, 965-978.

Brown, G. & Brindley, G.W. (1980): X-ray diffraction procedures for clay mineral identification. *In* Crystal Structures of Clay Minerals and their X-Ray Identification (G. Brown & G.W. Brindley, eds.). Spoottiswoode Ballantyne Ltd., Colchester and London, U.K. (305-359).

Galán, E., Carretero, M.I. & Fernandez-Calani, J.C. (1999): Effects of acid mine drainage on clay minerals suspended in the Tinto River (Rio Tinto, Spain). An experimental approach. *Clay Minerals* **34**, 99-108.

Henning, K.-H. & Störr, M. (1986): *Electron Micrographs (TEM, SEM) of Clays and Clay Minerals*. Akademie-Verlag, Berlin, Germany.

Hower, J. & Mowatt, T.C. (1966): The mineralogy of illites and mixed-layer illite/montmorillonites. *Am. Mineral.* **60**, 854-862.

Jambor, J.L. & Blowes, D.W. (1998): Theory and applications of mineralogy in environmental studies of sulfide-bearing mine wastes. *In* Modern Approaches to Ore and Environmental Mineralogy (L.J. Cabri & D.J. Vaughan, eds.). *Mineral. Assoc. Can., Short Course Vol.* **27**, 367- 401.

Johns, W.D., Grim, R.E. & Bradley, W.F. (1954): Quantitative estimations of clay minerals by diffraction methods. *J. Sed. Petrol.* **24**, 242-251.

Loucks, R.R. (1991): The bound interlayer H_2O content in potassic white micas: muscovite – hydromuscovite – hydropyrophilite solutions. *Am. Mineral.* **79**, 1563-1579.

Moore, D.M. & Reynolds, R.C., Jr. (1997): *X-ray Diffraction and the Identification and Analysis of Clay Minerals*. Oxford University Press, New York, N.Y.

Newman, A.C.D. & Brown, G. (1987): The chemical constitution of clays. *In* Chemistry of Clays and Clay Minerals (A.C.D. Newman, ed.). John Wiley and Sons, New York, N.Y. (1-129).

Nordstrom, D.K. (1982): The effect of sulfate on aluminum concentrations in natural waters: some stability relations in the system Al_2O_3–SO_3–H_2O at 298 K. *Geochim. Cosmochim. Acta* **46**, 681–692.

_____ & Ball, J.W. (1986): The geochemical behaviour of aluminum in acidified surface water. *Science* **232**, 54-56.

Ortiz, R.F., Von Guerard, P. & Walton-Day, K. (1995): Transport of metals into and through Terrace Reservoir, south-central Colorado, August 9–10, 1993. *In* Summitville Forum Proc. (H.H. Posey, J.A. Pendleton & D. Van Zyl, eds.). *Colorado Geol. Surv., Spec. Publ.* **38**, 178-182.

POUCHOU, J.L. & PICHOIR, F. (1984): Un nouveau modèle de calcul pour la microanalyse quantitative par spectrométrie de rayons X. I. Application à l'analyse d'échantillons homogènes. *Recherches Aérospatiales* **3**, 167-192.

SCHULTZ, L.G. (1958): Quantitative X-ray determinations of some aluminous minerals in rocks. *In* Clay and Clay Minerals (A. Swineford, ed.). Pergamon Press, New York, N.Y. (216-224).

_____ (1964): Quantitative interpretation of mineralogical composition from X-ray and chemical data for Pierre Shale. *U.S. Geol. Surv., Prof. Pap.* **391–C**.

SHAW, S.C. (2000): Geochemical characterization and water quality predictions for the Zortman/Landusky reclamation project. *In* Proc. of Mine Design, Operations & Closure Conf. (Polson, Montana).

_____ & ROBERTSON, A.M. (2001): Geochemical predictions of the Landusky spent ore heap-leach pads and implications for water management. *In* Metal Leaching and Acid Rock Drainage, Workshop Proc. (W.A. Price, ed.).

WALTON-DAY, K., ORTIZ, R.F. & VON GUERARD, P. (1995): Sources of water having low pH and elevated metal concentrations in the upper Alamosa River from the headwaters to the outlet of Terrace Reservoir, south-central Colorado, April–September, 1993. *In* Summitville Forum Proc. (H.H. Posey, J.A. Pendleton & D. Van Zyl, eds.). *Colorado Geol. Surv., Spec. Publ.* **38**, 171-177.

WILSON, M.R. & KYSER, T.K. (1988): Geochemistry of porphyry-hosted Au–Ag deposits in the Little Rocky Mountains, Montana. *Econ. Geol.* **83**, 1329-1346.

WITZKE, T. (1999): Hydrowoodwardite, a new mineral of the hydrotalcite group from the Konigswalde near Annaberg, Saxony/Germany and other localities. *Neues Jahrb. Mineral., Monatsh.*, 75-86.

Received October 10, 2003, revised manuscript accepted March 5, 2004.